

Structural and Electrochemical Characterization of Radio Frequency Magnetron-Sputtered LiCoO₂ Thin Films

Fabian Michel,* Marcel Couturier, Martin Becker, and Angelika Polity

LiCoO₂ thin films are grown by radio frequency magnetron sputter-deposition on platinum-coated Al₂O₃ (c-sapphire) substrates. Deposition parameters such as substrate temperature and the partial pressure ratio between O₂ and Ar are varied to find suitable parameters for a cathode offering reversible intercalation and deintercalation of lithium ions. Structural characterization is carried out using X-ray diffraction and Raman spectroscopy, revealing that the orientation as well as the crystallinity of the deposited LiCoO₂ films can be influenced by varying the O₂/Ar ratio and simultaneously applying a sufficient substrate temperature during deposition. Furthermore, both the atomic composition and the atomic distribution are determined using X-ray photoelectron spectroscopy and secondary ion mass spectrometry. Results show that the films possess surface contaminations of Li and oxygen-rich compounds but have a homogeneous atomic distribution throughout the depth profile. For electrochemical characterization, LiCoO₂ thin films were charged and discharged against lithium metal while using a liquid electrolyte consisting of LiPF₆ dissolved in a mixture of ethylene carbonate/dimethyl carbonate with a molar fraction of 1:1. Reversible discharge capacities in the order of up to 70 mAh g⁻¹ or 32.40 μAh cm⁻² μm⁻¹ can be achieved for optimized LiCoO₂ thin films.


density (125 Wh kg⁻¹, 440 Wh l⁻¹), the high reversible capacity (140 mAh g⁻¹), and an achievable battery voltage of over 4 V.^[1] However, due to the ever increasing energy needs of humanity, it is important to further increase the energy density and to continue to ensure or even improve the safety of the batteries. These ideas should be satisfied by the so-called all-solid-state-battery (solid-state battery), a battery made entirely of solid-state materials. Easy miniaturization, no leakage of electrolyte or ignition, and prolonged lifetime are the major advantages that result from the use of a solid electrolyte. In recent years, there has been a severe interest in the application of thin-film cathodes in microelectromechanical systems (MEMS), smart cards, or implantable medical devices. For example, a miniaturized solid-state battery should serve as a so-called “on-chip power supply element” and enable a direct emergency power supply.^[2] LiCoO₂ is an extremely promising cathode material due to its excellent electrochemical properties. To date, many

1. Introduction

As known, the rechargeable lithium-ion battery (LIB) is the most representative candidate when it comes to powering portable, electrical devices such as cell phones or laptops. LiCoO₂ proposed by Goodenough et al., was the first commercially used cathode material in such a LIB. Even today, LiCoO₂ is one of the most important cathode materials due to its high energy

studies have focused on LiCoO₂ thin-film cathodes fabricated using common techniques such as radio frequency (RF) magnetron sputtering,^[3–5] pulsed laser deposition,^[6,7] spray methods,^[8] sol–gel coating,^[9] and chemical vapor deposition.^[10,11] LiCoO₂ crystallizes in the rhombohedral high temperature (HT) or cubic low temperature (LT) phase, depending on the manufacturing conditions. In battery applications, the HT phase is preferred because of its suitable electrochemical properties such as increased capacity and better cycle stability compared with the LT phase. Furthermore, there is a desire to obtain the HT-LiCoO₂ film in a suitable orientation in growth direction, as the efficiency of the Li⁺ diffusion can be further enhanced. An overview of the properties of RF-sputtered LiCoO₂ is given by Julien et al.^[12] In this article, we will investigate the deposition of LiCoO₂ thin films via RF magnetron sputtering on heated platinum-coated c-sapphire substrates. Compared with the parameters given by Julien et al., we gain additional information about the thin film using a different substrate and deposition temperature. Structural characterization of the films was carried out as a function of the substrate temperature and the oxygen-to-argon ratio during the deposition. Elemental distribution of atomic compounds near the surface of optimized films was analyzed. Also the electrochemical performance of a LiCoO₂ film was evaluated.

Dr. F. Michel, M. Couturier, Dr. M. Becker, Dr. A. Polity
Institute for Exp. Physics I and Center for Materials Research (LaMa)
Justus-Liebig-University Giessen
Heinrich-Buff-Ring 16, 35392 Giessen, Germany
E-mail: fabian.michel@exp1.physik.uni-giessen.de

 The ORCID identification number(s) for the author(s) of this article can be found under <https://doi.org/10.1002/pssa.202000382>.

© 2020 The Authors. Published by Wiley-VCH GmbH. This is an open access article under the terms of the Creative Commons Attribution License, which permits use, distribution and reproduction in any medium, provided the original work is properly cited.

Correction added on 9 September 2020, after first online publication: Projekt Deal funding statement has been added.

DOI: 10.1002/pssa.202000382

2. Results and Discussion

2.1. Structure and Morphology

Figure 1a shows the growth rate of LiCoO₂ depending on the used O₂/Ar ratio at a present substrate temperature of 454 °C during deposition. Film thicknesses were determined using scanning electron microscopy (SEM) images of the breaking edges of the samples, cf. exemplary inset in Figure 1a. An increase in the growth rate (9–20 nm min⁻¹) can be observed when the O₂/Ar ratio is changed from 1:1 to 0:1.

As the working pressure was set constant at ≈0.1 Pa, the mean free path of particles was not influenced. The increasing growth rate with decreasing O₂/Ar ratio can thus simply be attributed to an increased amount of Ar ions, which are mainly responsible for the removal of atoms or clusters out of the LiCoO₂ target. Figure 1b shows a rather small increase in the growth rate (8–9 nm min⁻¹) when the substrate temperature is enhanced

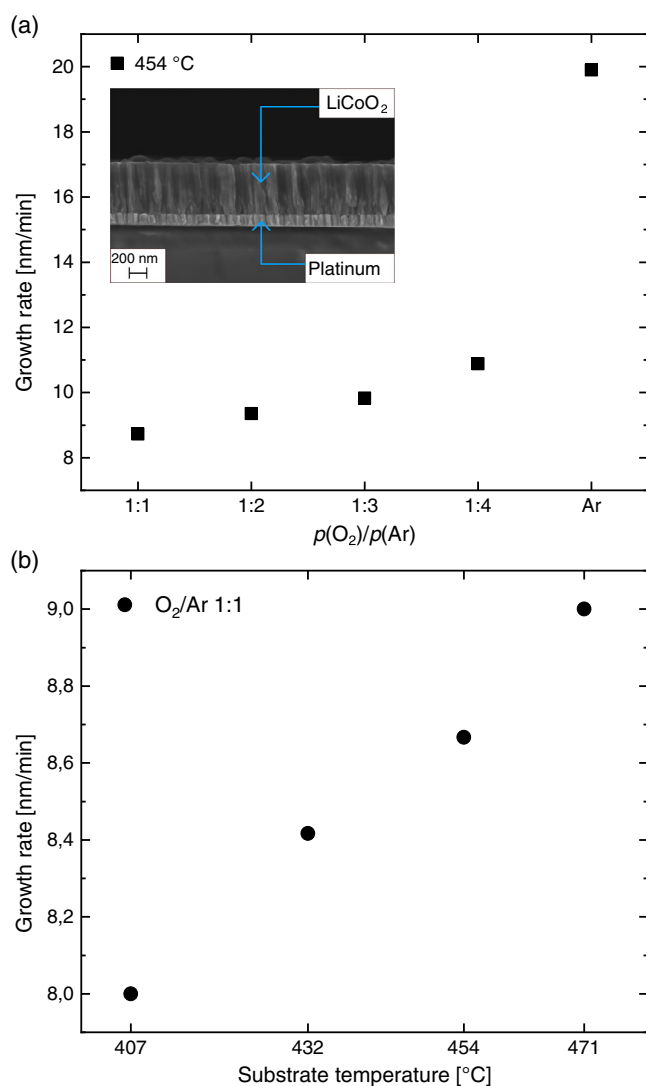


Figure 1. Growth rate of sputtered LiCoO₂ thin films with respect to the used a) O₂/Ar ratio and b) the substrate temperature during deposition.

from 407 up to 471 °C. Consequently, the increased kinetic energy of the film-forming particles led to increased film thicknesses. According to these results, desorption processes can most likely be excluded. Resulting thicknesses of the thin films for a sputter duration of 1 h at 454 °C are shown in Table 1. Figure 2a shows the Raman spectra of the LiCoO₂ thin films which were grown for 1 h under the different O₂/Ar partial pressure ratios while applying a constant substrate temperature of 454 °C. Factor-group analysis of the lattice vibrations in

Table 1. Film thicknesses of LiCoO₂ deposited at 454 °C for 1 h, depending on the O₂/Ar ratio used.

$p(\text{O}_2): p(\text{Ar})$	d (LiCoO ₂) [nm]
1:1	524
1:2	561
1:3	590
1:4	653
Ar	1195

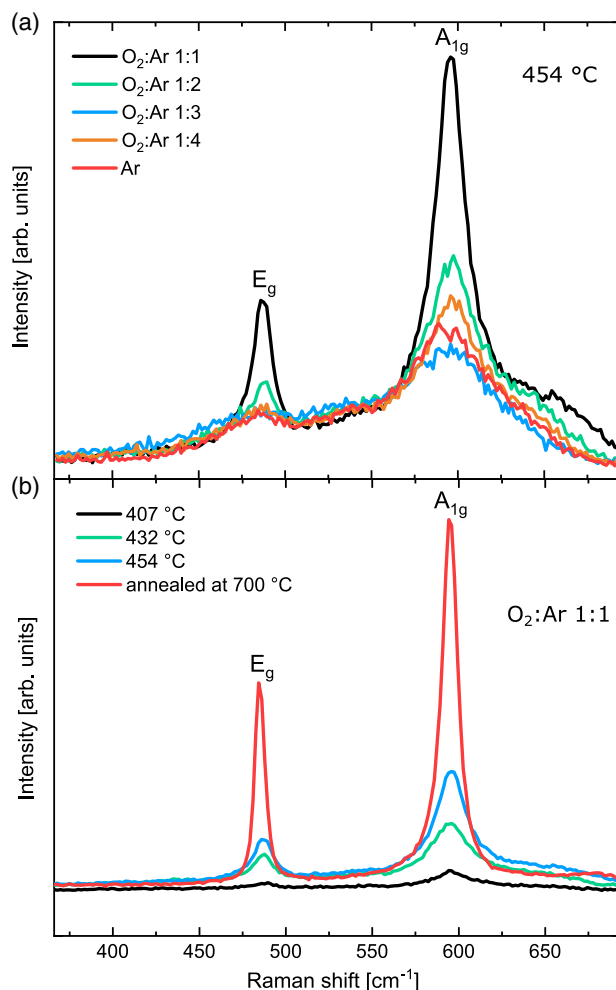


Figure 2. Raman spectra of LiCoO₂ films, a) deposited under different O₂/Ar ratios at 454 °C and b) deposited at different substrate temperatures at a constant O₂/Ar ratio of 1:1.

rhombohedral HT-LiCoO₂ with the space group $R\bar{3}m$ reveals two Raman active vibrational modes, A_{1g} and E_g. The A_{1g} and E_g modes are caused by the vibration of oxygen-atoms along the *c*-axis and along the *a*-*b* plane in the LiCoO₂ lattice, respectively.^[13] As shown in Figure 2a, the A_{1g} and E_g modes of HT-LiCoO₂ are observed at 595 and 488 cm⁻¹, respectively. With increasing proportion of oxygen in the sputter chamber during deposition, an increase in the modes intensity can be observed. Most likely an oxidation of the target surface occurs, suppressing the formation of Co₂O₄ and thus favoring the formation of LiCoO₂.^[14] Also it has to be considered that increasing the oxygen partial pressure can lead to an increase in the Li/Co ratio in LiCoO₂, as it was already observed by Liao et al.^[15]

In addition, a change of the absorption coefficient α takes place when the Li/Co ratio is changed.^[13] At a photon energy of 2.41 eV (514 nm), which was used during the Raman experiments, for $x = 0.87$ and $x = 0.53$ in Li_{*x*}COO₂, the resulting values for α are 0.16×10^6 and 0.34×10^6 cm⁻¹, respectively.^[16] The penetration depth of the laser can then be calculated to 62.5 nm for $x = 0.87$ and 29.4 nm for $x = 0.53$. The minimum film thickness for the examined LiCoO₂ films in Figure 2a is 524 nm. Consequently, the absorption coefficient α of LiCoO₂ films which were sputtered under high oxygen partial pressure might be increased thus leading to a detection of additional vibrational modes of oxygen atoms in deeper regions of these samples. Figure 2b shows the Raman spectra of LiCoO₂ thin films sputtered at different substrate temperatures as well as the spectra of a LiCoO₂ thin film postannealed at 700 °C. With increasing temperature, an increase in the A_{1g} and E_g modes can be observed, indicating a gain in crystallinity of the thin films. Through the postannealing, the formation of the HT-phase could be further improved. Raman modes of LT-LiCoO₂ and Co₂O₄ as determined experimentally by Mendoza et al. are not observed for the deposited films.^[17] In addition to Mendoza et al., a Raman study of LCO thin films is shown by Pan and Yang where a clear difference between the signal structure presented in there and the signal structure obtained from our samples is visible.^[18] However, there is no LT-LCO-related Raman mode visible for the very low pressure during deposition like it is known from Tintignac et al.^[19] According to the Raman results, LiCoO₂ thin films mainly consist of HT-LiCoO₂, if a homogeneous growth through the entire depth profile is assumed. While the formation of LT-LiCoO₂ during sputtering at a substrate temperature of 454 °C seems to be highly unlikely,^[20,21] the formation of Co₂O₄ might not be entirely excluded. A formation of Co₂O₄ at the interface between the substrate and the LiCoO₂ thin films could already be observed^[22] and is, because of the low penetration depth of the Raman laser, not detectable with our experimental Raman setup.

Figure 3a shows the X-ray patterns of the LiCoO₂ thin films deposited for 1 h under different O₂/Ar partial pressure ratios while applying a constant substrate temperature of 454 °C. Polycrystalline HT-LiCoO₂ and Co₂O₄ exhibit X-ray reflexes under nearly the same Bragg angles which makes it very difficult to distinguish between these two materials based on X-ray diffraction (XRD) results.^[19] According to the Raman results shown, the existence of Co₂O₄ in deeper regions of the sample can not be excluded. Thus, HT-LiCoO₂ as well as Co₂O₄ were considered for the XRD peak classification. The LiCoO₂ thin films show reflexes

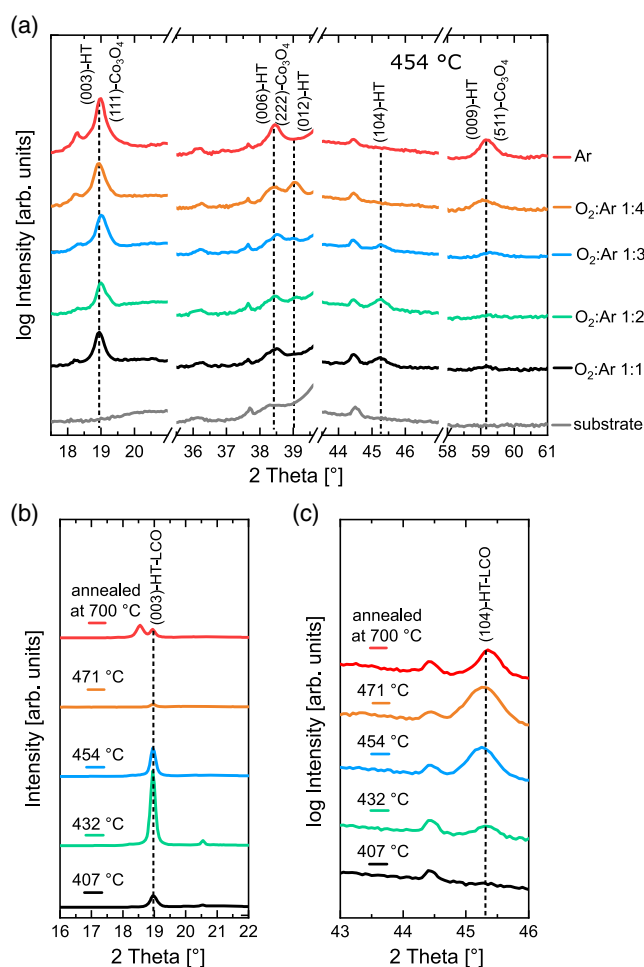


Figure 3. XRD spectra of LiCoO₂ thin films, a) deposited under different O₂/Ar ratios at 454 °C and b,c) deposited at different substrate temperatures at a constant O₂/Ar ratio of 1:1.

at angles of 19°, 38.5°, and 59.3°, respectively, which might either be attributed to (003)-oriented HT-LiCoO₂ in first, second, and third order or to (111)-, (222)-, and (511)-oriented Co₂O₄, cf. Figure 3a. Assuming these reflexes originate from Co₂O₄ might be meaningful especially for the thin films produced with less oxygen or even pure Ar, as a reducing environment can lead to the formation of Co₂O₄.^[14] Nevertheless with increasing the O₂/Ar ratio, an increase in the (104) orientation, favorable for LIBs, can be observed. Figure 3b,c shows the influence of the substrate temperature on the (003) and (104) peak intensities when sputtering occurred under an O₂/Ar ratio of 1/1. Excluding the film deposited at 407 °C, a decrease in (003) and an increase in (104) orientations with rising substrate temperature is observed. Optimized LiCoO₂ thin films were repetitively sputtered at a substrate temperature of 454 °C and an O₂/Ar ratio of 1/1, showing high-intensity Raman modes as well as a mixture of (003)- and (104)-oriented LiCoO₂ grains, i.e., a reproduction of the structural properties of the thin films could be achieved. The surface of an optimized film is shown in Figure 4 via SEM (Figure 4a) and via atomic force microscopy (AFM) (Figure 4b), revealing a dense layer of LiCoO₂ with atomic

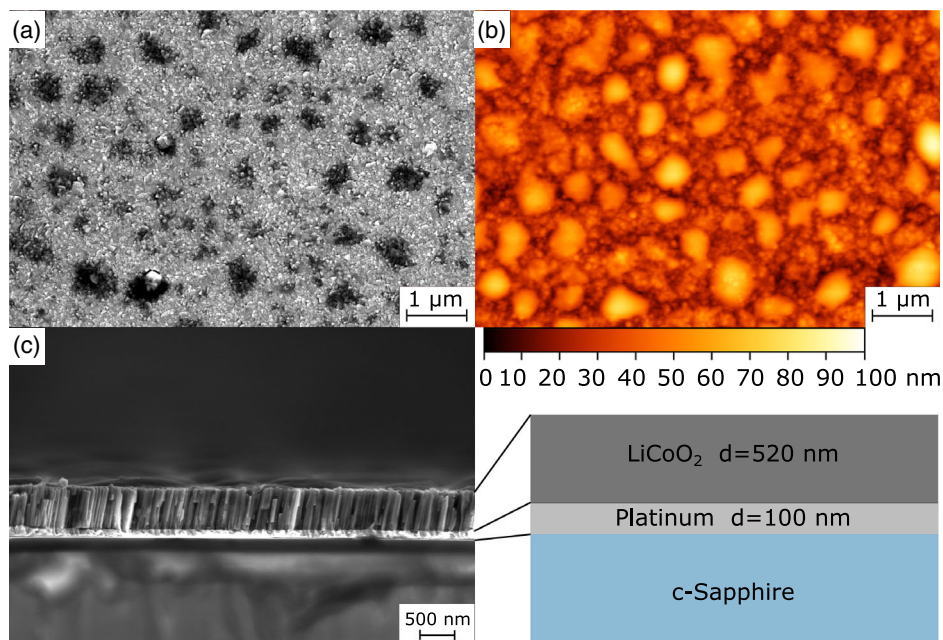


Figure 4. Surface morphology of an optimized LiCoO_2 thin film recorded via a) SEM and b) AFM and a cross section of the sample with the layer sequence c-sapphire|platinum| LiCoO_2 .

agglomerations with diameters of up to 400 nm on the surface. In a cross section of the thin film, a Volmer–Weber island growth mechanism of LiCoO_2 on platinum layer is visible, cf. Figure 4c. This growth mechanism was observed previously for LiCoO_2 sputtered onto a platinum layer.^[23] The surface agglomerations might be a consequence of the island growth mechanism and could be reduced with a reduction of the sputtering power and thus the growth rate. Yet, an average surface roughness of 8.2 nm could be estimated for the optimized LiCoO_2 film.

2.2. Phase Determination via X-Ray Photoelectron Spectroscopy

The X-ray photoelectron (XP) spectra of an optimized thin film are shown in Figure 5. In addition to the XP signal of the surface, three additional spectra were recorded, each after 120 s of Ar^+ -etching. Figure 5a shows the Co 2p core levels with its components $2p_{3/2}$ and $2p_{1/2}$ at binding energies of 780 and 795.5 eV

which arise as a result of the spin–orbit coupling. The accompanying satellite structures at 789 and 804 eV can be attributed to Co^{3+} , as it is expected for LiCoO_2 . The intensity of the Co 2p photoelectron signal is increased continuously when Ar^+ etching was accomplished, indicating the presence of phases without Co on the surface of the film. The O 1s spectrum of the film exhibits two peaks labeled O^{2-} surface and O^{2-} bulk at binding energies of 529 and 531.6 eV. O^{2-} bulk can be attributed to lattice oxygen in the LiCoO_2 network, whereas O^{2-} surface arises as a consequence of oxygen containing surface species such as LiCoO_2 , LiOH , and Li_2O .^[24] The Li 1s signal of the LiCoO_2 surface in Figure 5c occurs at a binding energy of 55 eV, whereas the Li 1s photoelectron of LiCoO_2 is expected to arise at binding energies of ≈ 54 eV.^[25,26] As already described for the O 1s signal, species Li_2CO_3 , LiOH , and Li_2O can be obtained within the Li 1s signal in the surface region of the thin film, shifting the signal to higher binding energies. For the C 1s spectrum of the analyzed film, three different types of carbon-containing

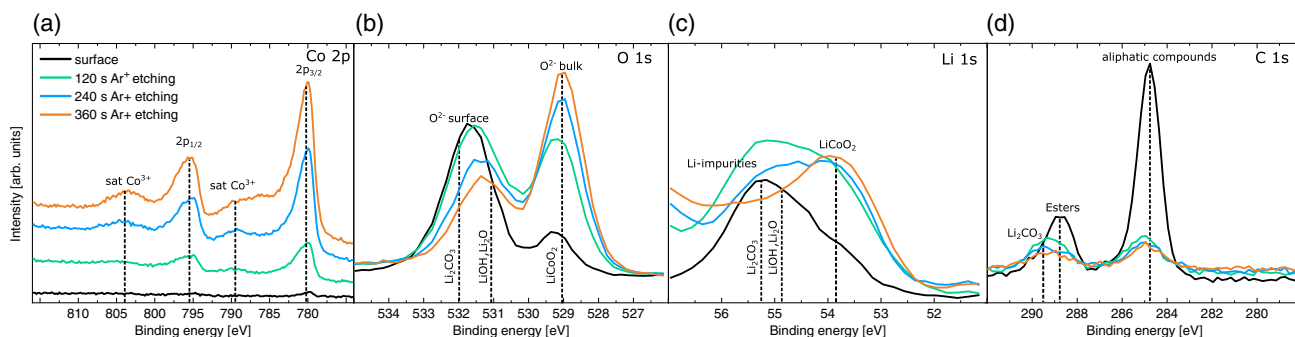


Figure 5. Photoelectron signals a) Co 2p, b) O 1s, c) Li 1s, and d) C 1s of the optimized LiCoO_2 thin film. In addition to the surface signal (black) three additional spectra (green, blue, and orange) were recorded, each after 120 s of Ar^+ etching.

species can be observed. A strong peak arises due to the contamination of the surface by aliphatic compounds at 284.8 eV. Furthermore, a contamination of esters as well as the already specified compound Li_2CO_3 are observed at binding energies of 288.9 and 289.6 eV, respectively. In summary, the LiCoO_2 thin films possess surface contaminations of Li_2CO_3 , LiOH , and Li_2O which are still detectable after 360 s of Ar^+ etching, implying that just a few nanometers of the thin film were removed by the etching process. These circumstances hinder a meaningful evaluation of the atomic concentration of Li, Co, and O in the LiCoO_2 thin film. Nevertheless, mass spectrum of the thin film was recorded via secondary-ion mass spectrometry (SIMS) to obtain the atomic relation between Co and Li, revealing a homogeneous distribution of Li and Co through the entire depth profile of the sample (not shown here).

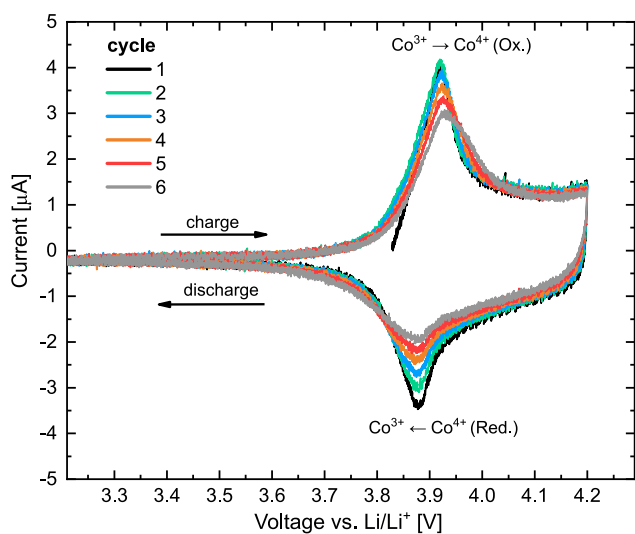


Figure 6. Cyclic voltammogram of the optimized LiCoO_2 thin film. The cyclic voltammogram was recorded using a sweep rate of 1 mV s^{-1} .

2.3. Electrochemical Characterization

The measured cyclic voltammogram of the electrochemical half cell containing the optimized LiCoO_2 thin film as a positive electrode is shown in **Figure 6**. The characteristic oxidation peak during charging can be observed at a voltage of 3.92 V versus Li/Li^+ . The reduction peak during the discharge occurs at 3.88 V, which yields a peak separation of about 40 mV characteristic for HT-LiCoO_2 .^[27]

The charge and discharge capacities of the electrochemical half cell containing the optimized LiCoO_2 thin film are shown in **Figure 7**. For calculating the mass of the 524 nm-thick LiCoO_2 film, the gravimetric density was estimated to be $\approx 4.5 \text{ g cm}^{-3}$ (90% of the literature value). Consequently, the used specific current of $11.6 \mu\text{A cm}^{-2}$ corresponded to a charge rate of 0.35. **Figure 7a** shows the charge curves of the cell for the first 20 cycles. The charge plateau is found to be at 3.9 V. The charge capacities reached for the different cycles can be read off at the intersections between curves and the upper axis of abscissae in units of mAh/g . While upon the first charge, a capacity of 72 mAh g^{-1} or $32.4 \mu\text{Ah cm}^{-2} \mu\text{m}^{-1}$ can be observed, the capacity continuously faded by 0.7% per cycle down to a value of 62 mAh g^{-1} or $27.9 \mu\text{Ah cm}^{-2} \mu\text{m}^{-1}$ for the 20th cycle. Discharging the cell for the first time delivered a discharge capacity of 70 mAh g^{-1} or $31.5 \mu\text{Ah cm}^{-2} \mu\text{m}^{-1}$. Cycling the cell delivered a capacity fading of 0.7% per cycle, similar to the behavior of the charge capacity. The corresponding Coulomb efficiency is $\approx 93\%$ for every charge/discharge cycle. The obtained discharge capacities of the first cycle are higher than for a sputter power optimized LCO thin film like it is shown in Jan et al.^[28] Although the discharge capacities in Zhu et al. are quite higher than for the thin films presented in this work, the Coulombic efficiency of 93% is higher in this case.^[29] However, the capacity fading in the publication of Zhu et al. is even bigger ($\approx 3.7\%$)^[29] than for the films reported in here ($\approx 0.7\%$). Most likely, this capacity fading is related to a degradation of the electrolyte used and might be further reduced by lowering this degradation. In

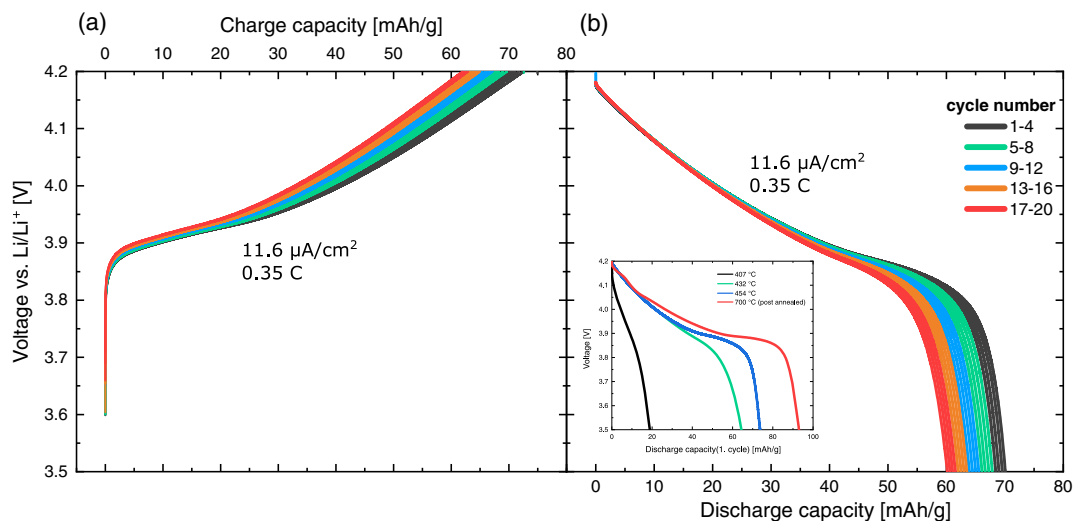


Figure 7. a) Charging and b) discharging curves of an electrochemical half cell including the optimized LiCoO_2 thin film. The cell with the sequence $\text{LiCoO}_2|\text{separator} + \text{LiPF}_6$ in $\text{EC/DMC}|\text{Li}$ was cycled over the voltage range of 3.5–4.2 V at a specific current of $11.6 \mu\text{A cm}^{-2}$ or rather 0.35 C.

Table 2. Deposition parameter and properties of the LCO thin films obtained in this work.

$p(\text{O}_2):p(\text{Ar})$	P [W cm^{-2}]	d_{LCO} [nm]	T [$^{\circ}\text{C}$]	Substrate	Discharge capacity	Structure
1:1	2.2	524	454	$\text{Al}_2\text{O}_3/\text{Pt}$	$32.40 \mu\text{Ah cm}^{-2} \mu\text{m}^{-1}$	(104)-orientation
1:1	2.2	524	700 (post annealed)	$\text{Al}_2\text{O}_3/\text{Pt}$	$41.85 \mu\text{Ah cm}^{-2} \mu\text{m}^{-1}$	(104)-orientation

addition, to the discharge curves of the optimized LiCoO_2 thin film, Figure 7b shows an inset showing the discharge curves of LiCoO_2 sputtered under different substrate temperatures as well as a postannealed LiCoO_2 film. One can observe that the substrate temperature leads to an increase in the discharge capacity. This can most likely be understood in terms of the higher crystallinity of these films, which allows a more efficient intercalation and deintercalation of Li^+ within the LiCoO_2 network. The highest discharge capacity of 93 mAh g^{-1} or $41.85 \mu\text{Ah cm}^{-2} \mu\text{m}^{-1}$ can be found for the electrochemical cell including the postannealed LiCoO_2 thin film. By post annealing a further increase in discharge capacity due to a almost higher crystallinity of the deposited films can be observed. So one has to decide if a higher deposition temperature or a postannealing step is suitable for production of high discharge capacity LCO material. If one compares the specific capacity of this work to the specific capacity of Tintignac et al.,^[19] the values obtained in our experiments are quite lower. This can be related to the fact that the deposition of our thin films was done at a working pressure of 0.1 Pa. An increase in specific capacity is related to an increase in pressure during deposition so the specific capacity of Tintignac et al. has to be higher because of the higher pressure during deposition (≈ 3 Pa). Tintignac et al. measured a specific capacity of $52 \mu\text{Ah cm}^{-2} \mu\text{m}^{-1}$ for 3 Pa and $22 \mu\text{Ah cm}^{-2} \mu\text{m}^{-1}$ for a deposition pressure of 0.55 Pa. However, the obtained value of $32.4 \mu\text{Ah cm}^{-2} \mu\text{m}^{-1}$ at 0.1 Pa and 454°C for the results presented in here is higher than the results shown in the study by Tintignac et al.^[19] at an increased deposition pressure. Regarding the review on RF-sputtered LCO thin films by Julien et al., a new substrate/thin-film combination at different substrate temperatures and Ar/ O_2 ratios was tested, obtaining a moderate discharge capacity of about $32.4 \mu\text{Ah cm}^{-2} \mu\text{m}^{-1}$ for the films deposited at substrate temperature of 454°C and $41.85 \mu\text{Ah cm}^{-2} \mu\text{m}^{-1}$ for the postannealed films.^[12] The experimental conditions and results are finally shown in Table 2.

3. Conclusion

The RF magnetron sputter deposition of LiCoO_2 thin films was successfully optimized by adjusting the deposition parameters such as substrate temperature and the oxygen-to-argon ratio in the plasma. Using a substrate temperature of 454°C and adding oxygen as a reactive gas to the deposition, the formation of rhombohedral HT- LiCoO_2 as well as (104)-orientated LiCoO_2 grains could be established. Best results were obtained for an O_2/Ar partial pressure ratio of 1:1 and a substrate temperature of 454°C , in terms of the most intense A_{1g} and E_g modes in Raman spectra and an increased proportion of (104)-orientated grains. Based on SEM images of the cross section of the samples, a Volmer–Weber growth of LiCoO_2 on platinum was detected.

As a result of this growth mechanism, particle agglomerations with diameters of up to 400 nm on the sample surfaces were observed. The average surface roughness was calculated to be 8.9 nm via AFM. XP spectra revealed impurity phases in the surface region such as Li_2CO_3 , Li_2O , and LiOH . After surface etching with Ar^+ ions, however, the signal Li 1s could be clearly assigned to LiCoO_2 . Electrochemical half cells with the layer sequence $\text{LiCoO}_2 \parallel \text{LiPF}_6$ in ethylene carbonate:dimethyl carbonate (EC:DMC 1:1 \parallel Li) were produced and successfully charged and discharged in a voltage range of 3.5–4.2 V versus Li/Li^+ . While cyclic voltammetry (CV) measurements approved the presence of HT- LiCoO_2 , cycling the cell at a specific current of $11.6 \mu\text{A cm}^{-2}$ or rather 0.35 C led to discharge capacities of 70 mAh g^{-1} or $31.5 \mu\text{Ah cm}^{-2} \mu\text{m}^{-1}$. A fade of the capacity of 0.7% per cycle was observed leading to a remaining capacity of 60 mAh g^{-1} or $27 \mu\text{Ah cm}^{-2} \mu\text{m}^{-1}$ after 20 cycles. Coulombic efficiency was observed to be constant at $\approx 93\%$.

4. Experimental Section

LiCoO_2 thin films were produced via RF magnetron sputtering. Stoichiometric LiCoO_2 with a purity of 99.7% from the company Kurt J. Lesker was used as sputtering target. c-Sapphire (Al_2O_3) was coated with a dense layer of 100 nm platinum and was used as a substrate. The platinum layer served as a current collector and was realized by an RF sputtering process of a metallic platinum target using 200 sccm Ar and a power density of 0.55 W cm^{-2} . For the deposition of the LiCoO_2 thin films, the substrate deposition temperatures (407, 432, 454, and 471°C), as well as the partial pressure ratio between the O_2 reactive gas and the Ar sputter gas (0:1, 1:1, 1:2, 1:3, and 1:4) were varied. A sputtering power density of 2.2 W cm^{-2} was applied to the LiCoO_2 target. In a prior work, the sputtering power and working pressure were determined as sufficient for these values. Also the optimal temperature range for our setup was identified at about $400\text{--}460^{\circ}\text{C}$. If one considers the temperature range of Zhu et al.,^[29] the temperature range in this work seems reasonable. The gas working pressure during deposition was set constant to 10^{-3} mbar. The substrate temperature was measured in advance, contacting the platinum surface of the substrates with a thermocouple while heating to the desired values. Raman spectroscopy was used to specify the thin films possible structural components such as LT- LiCoO_2 , HT- LiCoO_2 , and Co_2O_4 . Light with the wavelength of 514 nm was produced by an Ar-ion laser and focused to a $15.9 \mu\text{m}^2$ -sized spot on the thin-film surfaces, resulting in a power density of $\approx 84 \text{ mW } \mu\text{m}^{-2}$. The crystalline phase and the orientation of the produced thin films were examined by XRD in Bragg–Brentano geometry using a Siemens Bruker D5000. Aluminum $K\alpha$ radiation ($K\alpha = 1486 \text{ eV}$) was accelerated on the films surfaces, whereas the angle of incidence was changed with a rate of $2^{\circ}/\text{min}$. Information concerning the chemical bonds were determined via X-ray photoelectron spectroscopy (XPS) using a PHI VersaProbe. X-rays were produced using an Al-anode ($K\alpha = 1486 \text{ eV}$). Measurements were carried out with a source angle of 45° . All experiments were realized with charge neutralization on the sample surface, and all spectra were referenced to the carbon signal (C 1s) at 284.8 eV. Depth profiles were measured via in situ argon-ion etching with acceleration voltage of 1 kV. Atomic distribution of the films was determined by SIMS. The surface morphology, cross section, and thus the

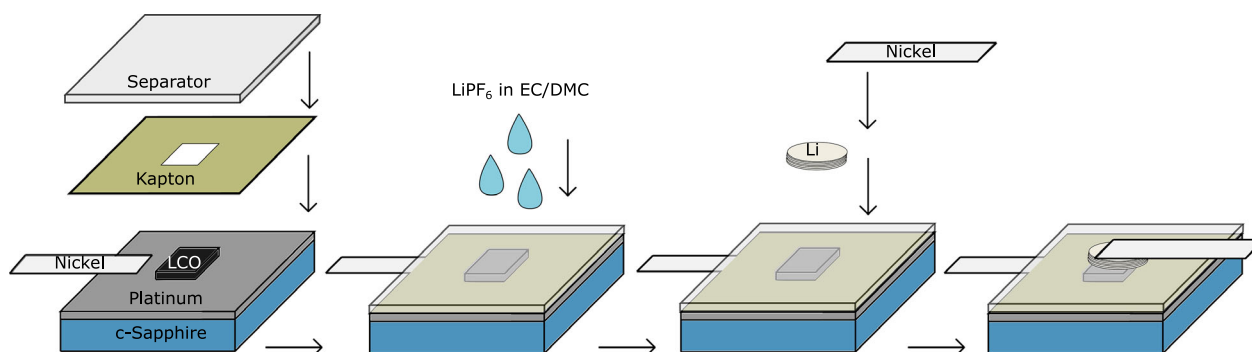


Figure 8. Schematic representation for the construction of electrochemical half cells with the sequence $\text{LiCoO}_2|\text{separator} + \text{LiPF}_6 \text{ in EC/DMC}|\text{Li}$.

thickness of thin films were examined by SEM using a Zeiss-Merlin setup. Surface roughness was evaluated utilizing AFM. For LiCoO_2 cathodes with a defined electrode area, substrates were provided with a temperature stable ceramic mask during the LiCoO_2 sputter deposition, resulting in electrode areas of $6 \times 5 \text{ mm}^2$. Electrochemical half cells were then assembled following the scheme in **Figure 8**. Fiberglass filters served as a separator and 1 M LiPF_6 in EC/DMC (1:1 by vol%) was used as the electrolyte. The charge/discharge testing and CV measurements were carried out using a VMP300 potentiostat. The cells were cycled over the voltage range of 3.5–4.2 V at a specific current of $11.6 \mu\text{A cm}^{-2}$ or rather 0.35 C. For CV measurements, a sweep rate of 1 mV s^{-1} was used.

Acknowledgements

Financial support was provided by the DFG via GRK (Research Training Group) 2204 “Substitute Materials for Sustainable Energy Technologies.” Open access funding enabled and organized by Projekt DEAL.

Conflict of Interest

The authors declare no conflict of interest.

Keywords

cathode materials, electrochemical properties, LiCoO_2 , sputter deposition

Received: June 22, 2020

Revised: June 30, 2020

Published online: August 31, 2020

- [1] T. Ohzuku, Y. Makimura, *Chem. Lett.* **2001**, 30, 642.
- [2] J.-K. Park, *Principles and Applications of Lithium Secondary Batteries*, Wiley-VCH, Weinheim, Germany **2012**.
- [3] D. Lin, Y. Liu, W. Chen, G. Zhou, K. Liu, B. Dunn, Y. Cui, *Nano Lett.* **2017**, 17, 3731.
- [4] M. Yamamoto, Y. Terauchi, A. Sakuda, M. Takahashi, *Sci. Rep.* **2018**, 8, 1212.
- [5] V. Thangadurai, D. Pinzaru, S. Narayanan, A. K. Baral, *J. Phys. Chem. Lett.* **2015**, 6, 292.

- [6] J. Cho, Y. J. Kim, B. Park, *Chem. Mater.* **2000**, 12, 3788.
- [7] M. N. Obrovac, V. L. Chevrier, *Chem. Rev.* **2014**, 114, 11444.
- [8] M. M. Thackeray, W. I. F. David, P. G. Bruce, J. B. Goodenough, *Mater. Res. Bull.* **1983**, 18, 461.
- [9] D. Aurbach, M. D. Levi, K. Gamulski, B. Markovsky, G. Salitra, E. Levi, U. Heider, L. Heider, R. Oesten, *J. Power Sources* **1999**, 8182, 472.
- [10] R. Korthauer, *Handbuch Lithium-Ionen-Batterien*, Springer Berlin Heidelberg, Germany **2013**.
- [11] C.-Z. Zhao, P.-Y. Chen, R. Zhang, X. Chen, B.-Q. Li, X.-Q. Zhang, X.-B. Cheng, Q. Zhang, *Sci. Adv.* **2018**, 4, eaat3446.
- [12] C. M. Julien, A. Mauger, O. M. Hussain, *Materials* **2019**, 12, 2678.
- [13] Y. Matsuda, N. Kuwata, T. Okawa, A. Dorai, O. Kamishima, J. Kawamura, *Solid State Ionics* **2019**, 335, 7.
- [14] J. Trask, A. Anapolsky, B. Cardozo, E. Januar, K. Kumar, M. Miller, R. Brown, R. Bhardwaj, *J. Power Sources* **2017**, 350, 56.
- [15] C.-L. Liao, Y.-H. Lee, K.-Z. Fung, *J. Alloys Compd.* **2007**, 436, 303.
- [16] H. L. Liu, T. Y. Ou-Yang, H. H. Tsai, P. A. Lin, H. T. Jeng, G. J. Shu, F. C. Chou, *New J. Phys.* **2015**, 17, 103004.
- [17] L. Mendoza, R. Baddour-Hadjean, M. Cassir, J. P. Pereira-Ramos, *Appl. Surf. Sci.* **2004**, 225, 356.
- [18] H. Pan, Y. Yang, *J. Power Sources* **2009**, 180, 633.
- [19] S. Tintignac, R. Baddour-Hadjean, J.-P. Pereira-Ramos, R. Salot, *Electrochim. Acta* **2012**, 60, 121.
- [20] H. Porthault, R. Baddour-Hadjean, F. Le Cras, C. Bourbon, S. Franger, *Vib. Spectrosc.* **2012**, 62, 152.
- [21] D. Depla, S. Mahieu, *Reactive Sputter Deposition*, Springer Series in Materials Science, Vol. 109, Springer, Berlin and Heidelberg, Germany **2008**.
- [22] T. Sander, *PhD Dissertation*, JLU-Giessen **2015**.
- [23] Y. Zhang, C. Chung, M. Zhu, *Rare Met.* **2008**, 27, 266.
- [24] K. Kanamura, H. Tamura, S. Shiraishi, Z.-I. Takehara, *Electrochim. Acta* **1995**, 40, 913.
- [25] L. Daheron, H. Martinez, R. Dedryvere, I. Baraille, M. Menetrier, C. Denage, C. Delmas, D. Gonbeau, *J. Phys. Chem. C* **2009**, 113, 5843.
- [26] N. Schulz, R. Hausbrand, L. Dimesso, W. Jaegermann, *J. Electrochem. Soc.* **2018**, 165, A819.
- [27] D. Ensling, *PhD Dissertation*, TU-Darmstadt **2006**.
- [28] D.-J. Jan, C.-C. Lee, Y.-J. Yu, H.-W. Chiang, *Jpn. J. Appl. Phys.* **2019**, 58, 085501.
- [29] X. Zhu, Z. Guo, G. Du, P. Zhang, H. Liu, *Surf. Coat. Technol.* **2010**, 204, 1710.